Journal of Medicinal Chemistry

Article

Molecular dynamics simulations and structure-based rational design lead to allosteric HCV NS5B polymerase thumb pocket 2 inhibitor with picomolar cellular replicon potency.

Oliver Thomas Hucke, René Coulombe, Mégan Bertrand-Laperle, Christian Brochu, James Gillard, Marc-André Joly, Serge Landry, Olivier Lepage, Martin Marquis, Ginette McKercher, Marc Pesant, Martin Poirier, Pierre L. Beaulieu, Pierre R Bonneau, Montse Llinàs-Brunet, George Kukolj, and Timothy A. Stammers

J. Med. Chem., **Just Accepted Manuscript** • DOI: 10.1021/jm4004522 • Publication Date (Web): 17 Jun 2013

Just Accepted

Journal of Medicinal Chemistry is published by the American Chemical Society. 1155 Sixteenth Street N.W., Washington, DC 20036

Title: Molecular dynamics simulations and structure-based rational design lead to allosteric HCV NS5B polymerase thumb pocket 2 inhibitor with picomolar cellular replicon potency.

Authors: Oliver Hucke, René Coulombe, Pierre Bonneau, Mégan Bertrand-Laperle, Christian Brochu, James Gillard, Marc-André Joly, Serge Landry, Olivier Lepage, Montse Llinàs-Brunet, Marc Pesant, Martin Poirier, Maude Poirier, Ginette McKercher, Martin Marquis, George Kukolj, Pierre L. Beaulieu and Timothy A. Stammers*

Authors address: Research and Development, Boehringer Ingelheim (Canada) Ltd., 2100 Cunard Street, Laval, Quebec, H7S 2G5, Canada

ABSTRACT

The design and preliminary SAR of a new series of 1H-quinazolin-4-one (QAZ) allosteric HCV NS5B thumb pocket 2 (TP-2) inhibitors was recently reported. To support optimization efforts, a Molecular Dynamics (MD) based modeling workflow was implemented, providing information on QAZ binding interactions with NS5B. This approach predicted a small but critical ligand-

binding induced movement of a protein backbone region which increases the pocket size and improves access to the backbone carbonyl groups of Val 494 and Pro 495. This localized backbone shift was consistent with key SAR results and was subsequently confirmed by X-ray crystallography. The MD protocol guided the design of inhibitors, exploiting novel H-bond interactions with the two backbone carbonyl groups, leading to the first thumb pocket 2 NS5B inhibitor with picomolar antiviral potency in genotype (gt) 1a and 1b replicons (EC_{50} = 120 pM and 110 pM, respectively), and with $EC_{50} \leq 80$ nM against gt 2-6.

INTRODUCTION

With an estimated 2-3% of the world population (130-170 million people; 5 million in the US alone) as chronic carriers of the Hepatitis C virus (HCV),[1] the impact of this infectious agent on public health is undeniable. Chronic HCV infection is a leading cause for hepatocellular carcinoma and liver transplants and causes approximately 86000 deaths/year worldwide.[2]

Until recently, the standard of care (SoC) for HCV treatment combined pegylated interferon-α (PegIFN) with the broad spectrum antiviral ribavirin (RBV). However, sustained viral responses (SVR) for this therapy rarely exceeded 50% for genotype 1 (gt1) the most prevalent genotype in North America, Europe and Japan. This limited efficiency, along with severe side effects,[3] underline the need for more efficacious and better tolerated approaches for HCV treatment.

Small molecules that specifically target HCV proteins (direct acting antivirals, DAAs) have now begun to address the need for improved treatment outcome and tolerability. An initial landmark in this regard was the structure-based peptidomimetic design of ciluprevir, the first inhibitor of a viral protein, in this case the HCV NS3/4A protease, to show antiviral activity in HCV infected patients.[4] Following this discovery, the search for NS3/4A inhibitors became a focus of HCV drug development for many pharmaceutical companies. Two agents from this class, boceprevir[5] from Merck and telaprevir from Vertex[6] have been approved. Today's new SoC (NSoC) combines one such protease inhibitor with the previously used PegIFN/RBV therapy. This new regimen improves SVR rates to 68-75% and shortens duration of treatment for some gt1 patients,[7] but still suffers from side effects associated with the PegIFN/RBV in addition to those caused by the new drugs themselves. Second generation HCV protease inhibitors with improved profiles are currently in clinical trials and are expected to reach market approval in the

near future (e.g. simeprevir[8] from Johnson & Johnson and faldaprevir from Boehringer Ingelheim[9]). However, these single DAA-based therapies still require combination with PegIFN/RBV in order to prevent rapid emergence of resistant virus. Future directions that could avoid the use of PegIFN and RBV co-therapy are therefore of high interest. Combining DAAs with complementary modes of action is one potential route to achieve this goal, and more recently multiple DAA combinations have indeed shown the potential to increase cure rates up to >90% in the gt1 population.[10]

HCV protease inhibitor faldaprevir and HCV NS5B polymerase inhibitor BI 207127 that binds to the allosteric thumb pocket 1 site (Fig. 1)are two DAAs from our portfolio currently under phase 3 clinical investigation in an IFN-free combination.[11] The thumb domain of NS5B also harbors a second allosteric pocket (thumb pocket 2, TP-2), where binding of ligands can also lead to inhibition of enzymatic function.[13] Although the exact molecular mechanisms by which allosteric NS5B pocket 1 and pocket 2 inhibitors disrupt RNA synthesis is not entirely defined, biochemical experiments suggest that they inhibit at the initiation stage of the RNA polymerization process by preventing the formation of a productive polymerase:RNA primer-template complex. It is generally assumed that inhibition of RNA synthesis occurs through interference with essential enzyme conformational changes.[13] Importantly, it has been shown *in vitro* that TP-1 and TP-2 NS5B inhibitors are not mutually exclusive, opening the possibility for new combinations of DAAs for HCV therapy.

We recently reported the fragment-based design of an anthranilic acid-based series of thumb pocket 2 NS5B inhibitors,[15] exploiting structural information on a bound fragment hit in conjunction with publicly available information on TP-2 binders. Subsequently we were able to use our knowledge of the anthranilic acid SAR and their binding mode to develop a structurally

novel, quinazolinone (QAZ) TP-2 chemotype (e.g. **1**, Figure 1) with a distinct physicochemical profile.[16]

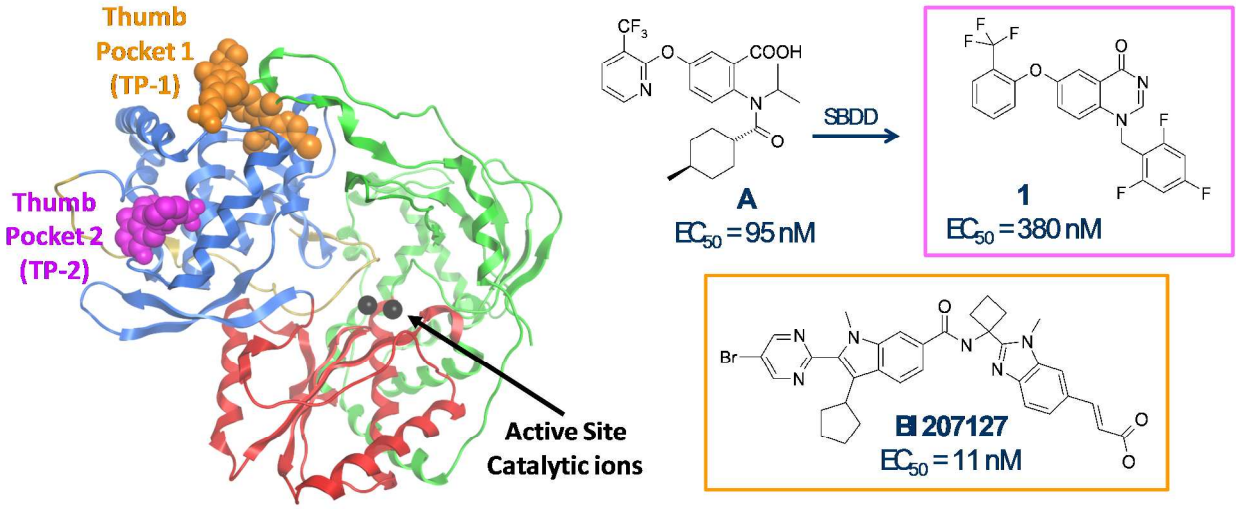

Figure 1 Ribbon structure of NS5B with thumb pockets 1 and 2 highlighted by two inhibitors (CPK representation). The depicted ligands are BI 207127 (TP-1, orange; model based on an in house X-ray structure with a related inhibitor) and QAZ type compound **1** (TP-2, magenta) that emerged from the anthranilic acid chemotype (exemplified by **A**) through structure based drug design (SBDD).[16] The NS5B palm domain is shown in red. It harbors the active site including two magnesium ions. The thumb domain (blue) contains a GTP binding site in close proximity to TP-1, which may be implicated in *de novo* initiation. The finger domain with the Λ finger loops (green) are forming a channel that holds the RNA in place and regulate replication.[12]

Herein, we describe the optimization of this quinazolinone TP-2 chemotype by extending protein-ligand interactions within the left hand side (LHS) region of the binding site, i.e. into the surface cleft above Leu 489 towards Val 494. (Fig. 2). A modeling approach using molecular

dynamics (MD) simulations that captured binding site flexibility, revealed a small but significant backbone conformational change that resulted in improved access to the carbonyl groups of Val 494 and Pro 495 and to extended hydrophobic interactions. The design of an analog exploiting these new interactions resulted in one of the most potent NS5B inhibitors reported to date, with picomolar potency in gt1 replicon assays and low nanomolar potency against gt 2-6.

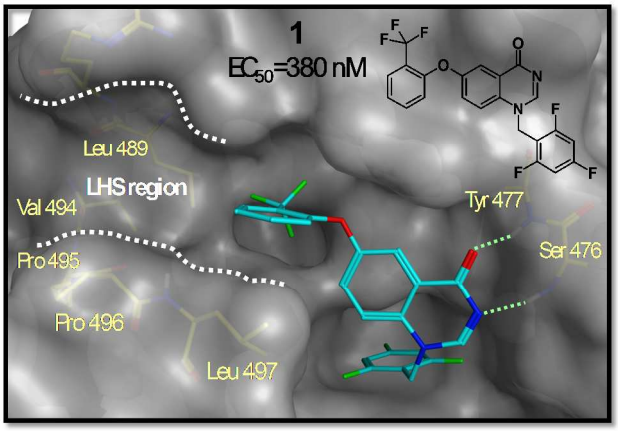

Figure 2 X-ray structure of quinazolinone (QAZ) **1** bound to TP-2 of HCV NS5B. This chemotype was designed to maintain H-bond interactions with the backbone NH groups of Ser 476 and Tyr 477 (green dashed lines).[16] White dashed lines outline the LHS region of TP-2 that was targeted for further optimization of the QAZ chemotype.

RESULTS AND DISCUSSION

Using our established X-ray crystallographic protocols (see Experimental section), we were able to determine the binding mode of a quinazolinone analog in complex with NS5B (Fig. 2). Compound **1** shows the expected H-bonds to the backbone NH groups of Ser 476 and Tyr 477 that are crucial for binding of the anthranilic acid series and other TP-2 NS5B inhibitors, and that

the quinazolinone core was designed to maintain.[16] The N^1-2,4,6-trifluorobenzyl group anchors the inhibitor by occupying a deep hydrophobic pocket while the (2-trifluoromethyl-)phenyl moiety at the other end of the molecule contacts the side chain of Leu 497 and places its CF_3 group in a small hydrophobic pocket. As depicted in Figure 2, a NS5B TP-2 surface cleft extends from the LHS portion of the inhibitor and can be engaged through additional substitutions on the LHS phenyl ring. This mostly hydrophobic LHS region of TP-2 was targeted to further improve the potency of the quinazolinone NS5B inhibitors.

The addition of an amide group at position 3 of the LHS phenyl ring slightly improved antiviral potency from 380 nM (compound **1**) to 180 nM (compound **2**; Table 1),[17] in spite of the increased hydrophilicity associated with the amide group, which may have negatively affected cell permeability. A more substantial gain in antiviral potency to the single digit nanomolar range was achieved by adding a phenyl or pyridyl substituent to the amide nitrogen atom (compounds **3**, **4**, **5** in Table 1). The X-ray structures of compounds **2** and **4** in complex with NS5B were solved by crystal soaking (Figure 3A), revealing in both cases a new hydrogen bond between the amide carbonyl group and the backbone NH of Leu 497. In fact, previous SAR and corresponding in-house X-ray structures of NS5B:TP-2 inhibitor complexes had shown that this H-bond interaction usually contributed to improved potency. Based on the high potency of **4** and related structures, subsequent SAR focused on maintaining the interaction with Leu 497 for productively exploring the LHS region of pocket 2. Interestingly, the LHS pyridine ring of compound **4** also forms a H-bond with the side chain of Arg 490 (Fig. 3A). However, compound **3**, which lacks the pyridyl nitrogen hydrogen bond acceptor, has comparable potency to compound **4** (Table 1), suggesting that the H-bond interaction with the Arg 490 side chain does not significantly contribute to activity. Indeed, multiple X-ray structures of NS5B reveal various

conformations of the side chain of Arg 490, and suggest that a potential gain in binding enthalpy through a hydrogen bond to its guanidino function may be offset by a loss in receptor entropy. Figure 3A also shows the high degree of conservation of the loop backbone structures of the Val 494 to Leu 497 region that was characteristic of all X-ray structures of NS5B:pocket 2 inhibitor complexes solved to date in both the anthranilic acid as well as quinazolinone chemotypes. The addition of the LHS amide group in compounds **2-5** resulted in a significant drop in apical to basolateral (A → B) Caco-2 cell permeability (Table 1), an effect often associated with amide groups and the presence of hydrogen-bond donors. In order to address this issue, an azabenzoxazole heterocycle was designed to mask the amide moiety while maintaining the H-bond acceptor in a position equivalent to the carbonyl oxygen atom of the amide group, suitable for forming a H-bond interaction with Leu 497.

Table 1 Early examples of LHS SAR exploration

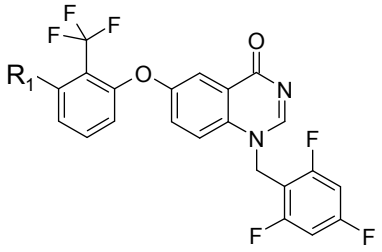

R_1	H		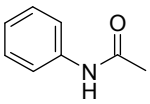	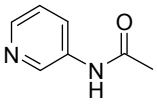	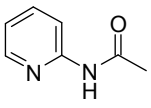	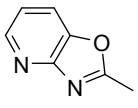

Compound	**1**	**2**	**3**	**4**	**5**	**6**
EC_{50} [a] (nM)	380±90	180±100	2.5±0.4	5.7±0.6	6.8±0.7	3.3±1.4
CACO-2[b] (10^{-6} cm/s)	9.2	1.9	0.84	0.26	1.2	3.0

[a] HCV gt 1b replicon luciferase reporter assay (n≥2).[18] [b] The Caco-2 permeability assay was run with apical pH 6.0/basolateral pH 7.4.

Prior to the synthesis of **6**, we evaluated our hypothesis with a simple model derived from the X-ray structure of NS5B with compound **4** bound to TP-2 (Figure 3B). This tentative model strongly suggested that formation of the H-bond between the oxazole nitrogen atom of **6** and Leu 497 would inevitably lead to a clash between the pyridine ring of the azabenzoxazole moiety and the backbone atoms of Pro 496 (Figure 3B). Attempts to resolve this clash through minimizations of **6** in a flexible protein binding site led to shifts of the LHS part of the inhibitor from the position shown in Figure 3B, away from Leu 497 and Pro 496, which caused a loss of the H-bond interaction. Unexpectedly, **6** maintained the high potency of compounds **3**-**5** and some improvement in Caco-2 cell permeability was also achieved, as intended by the design (Table 1). The discrepancy between the observed potency of **6**, the available structural information on this class of inhibitors and initial modeling results prompted the use of X-ray crystallography to gain further experimental information on the binding mode and rationalize the potency achieved with this class of compounds. Unfortunately, repeated attempts to soak **6** into NS5B crystals using our established procedures (see Experimental section) were unsuccessful. Severe crystal cracking was observed upon soaking of compound **6**, and suggested possible ligand-induced protein conformational changes or disturbance of crystal packing. In the absence of X-ray information, we turned to a molecular dynamics (MD) based modeling protocol that accounted for protein flexibility to elucidate the binding geometry of **6**. In this structure prediction protocol, the thumb domain that harbors pocket 2 was considered (220 residues) with all amino acid residues fully flexible, except those that are at the interface with the parts of NS5B which were not considered in the simulation (38 restrained residues, 17% of the residues

considered; Figure 5 summarizes the simulation approach; See Experimental section and supporting information for additional details).

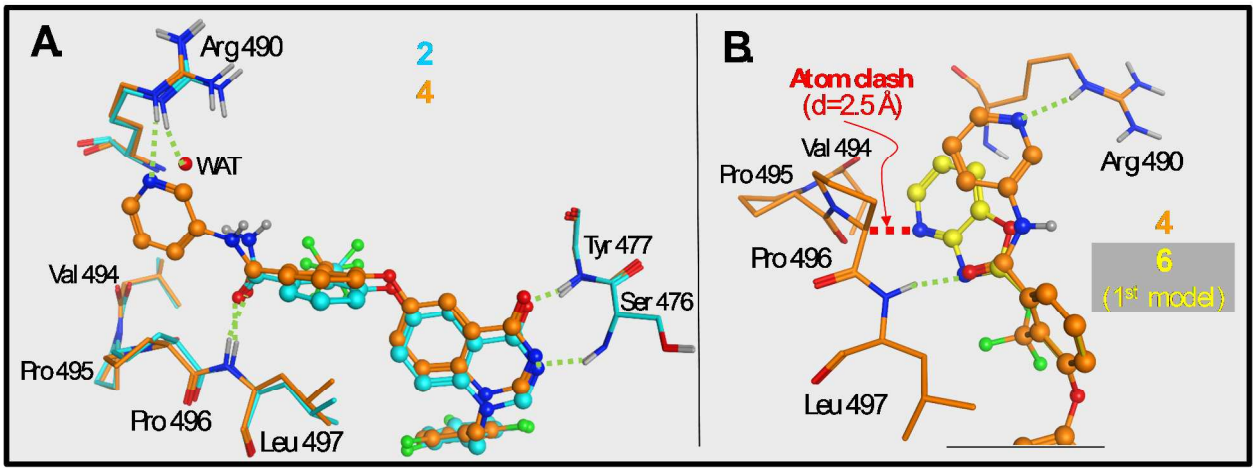

Figure 3, A. Superposition of the X-ray structures of the binding modes of **2** and **4**. The LHS amide carbonyl group forms a H-bond with the backbone NH of Leu 497. The LHS pyridine ring of **4** displaces a water molecules that, in the X-ray structure with **2**, forms a H-bond with the side chain of Arg 490. (The H-bond between **4** and Arg 490 does not contribute to antiviral potency, as suggested by the comparable potency of compound **3**); **B.** X-ray binding mode of **4** (different perspective, otherwise identical to A) superposed with a first tentative model of the binding mode of **6,** obtained by modifying **4** in its bound conformation. A H-bond between **6** and the backbone NH of Leu 497 inevitably leads to a serious atom clash with Pro 496.

The binding mode of **6** predicted using the MD protocol is shown in Figure 4A, in superposition with the X-ray structure of **4** bound to TP-2. The overall binding geometries of compounds **4** and **6** are highly similar, with the oxygen atom of the oxazole part of the LHS bicyclic ring system of **6** mimicking the amide carbonyl oxygen atom of **4**. However, no hydrogen bond between **6** and the NH of Leu 497 is observed. The absence of this interaction is due to a unique conformation of the loop region between Val 494 and Leu 497. This backbone

region shifts relative to the usually observed crystallographic position by approximately 1 Å such that the clash between Pro 496 and the leftmost pyridine ring of **6** is avoided. One consequence of this conformational change is that the backbone NH of Leu 497 points away from the oxazole ring, above the plane of the azabenzoxazole system, where there is space for interaction with a water molecule. In addition to avoiding the clash with Pro 496 this alternate protein conformation improves access to the backbone carbonyl groups of Pro 495 and Val 494 which form favorable electrostatic contacts with two C-H groups of the pyridine ring in our model. These are highly polarized due to the electron withdrawing effect of the nitrogen and oxygen atoms of the heterocycle and are thus suitable for such polar interactions and likely contribute to the improved potency of **6**.

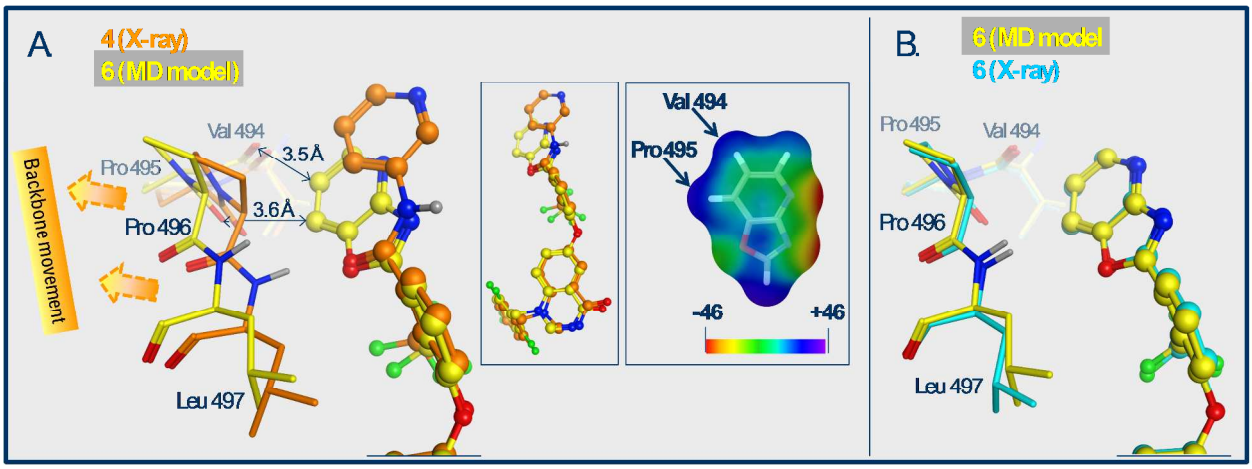

Figure 4 A. Binding mode of **6** as predicted by the MD protocol in comparison with compound **4** (X-ray structure): The binding of **6** induces a shift of the protein backbone between Val 494 and Leu 497, leading to favorable C-H…O contacts with the backbone carbonyl groups of Val 494 and Pro 495 (arrows – distances are indicated). No H-bond to Leu 497 is apparent for compound **6**. Only the variable LHS portions of the two inhibitors are shown for clarity. The insets show good overall agreement of the bound geometries of both compounds and the electrostatic surface potential (ESP) of the azabenzoxazole group (ESP units: kcal/mol; Arrows indicate CH groups

contacting the carbonyls of Val 494 and Pro 495). **B**. Comparison of binding modes of **6** predicted by the MD simulation protocol (yellow) and observed in a subsequently obtained X-ray structure (cyan). The root mean square deviation (rmsd) between the model and X-ray structure amounts to 0.48 Å for the loop residues Val 494 – Leu 497 and to 0.31 Å for the ligand atoms (rmsd based on non-hydrogen atoms; only LHS portion of ligand shown, for clarity – all ligand atoms were considered in the rmsd calculation). Superpositions were done using the C_α atoms of the thumb domain.

In an effort to acquire an X-ray structure of NS5B with compound **6** bound to TP-2, a variety of soaking conditions were screened and optimized to provide a 3.0 Å resolution X-ray model. The superposition of the MD model with the experimentally derived X-ray structure shows excellent agreement (Figure 4B): It fully confirmed the predicted bound geometry of the inhibitor as well as the localized shift of the protein backbone. (Based on the relatively low resolution of this X-ray structure an orientation of the azabenzoxazole group that is rotated by 180° can not be excluded. However, in this rotated orientation both nitrogen atoms would point towards the protein, causing desolvation and electrostatic repulsion with the backbone carbonyl of Pro 495. This orientation was therefore considered unlikely).

This concordance of prediction and experiment further validated the MD protocol and it was subsequently used to guide chemistry efforts through structure-based interpretation of SAR and the creation and assessment of design ideas prior to synthesis. To allow a more efficient use of this approach, different steps of the MD workflow were automated, such that simulations for different hypothetical poses of the same inhibitor in TP-2 or for a set of different inhibitors were set up and submitted to a Linux cluster and results were retrieved in an automated fashion. (Figure 5; see Experimental section for details). The MD protocol included distance restraints

that favored the presence of the H-bond interactions between the quiazolinone core and the backbone NH groups of Ser 476 and Tyr 477. These restraints were based on previous SAR that showed that these interactions were crucial for potency and they were at the heart of the structure based design leading to the quinazolinone chemotype.[16] The restraints were applied to focus the MD sampling on the LHS region of the inhibitors that was the focus of ongoing synthesis efforts.

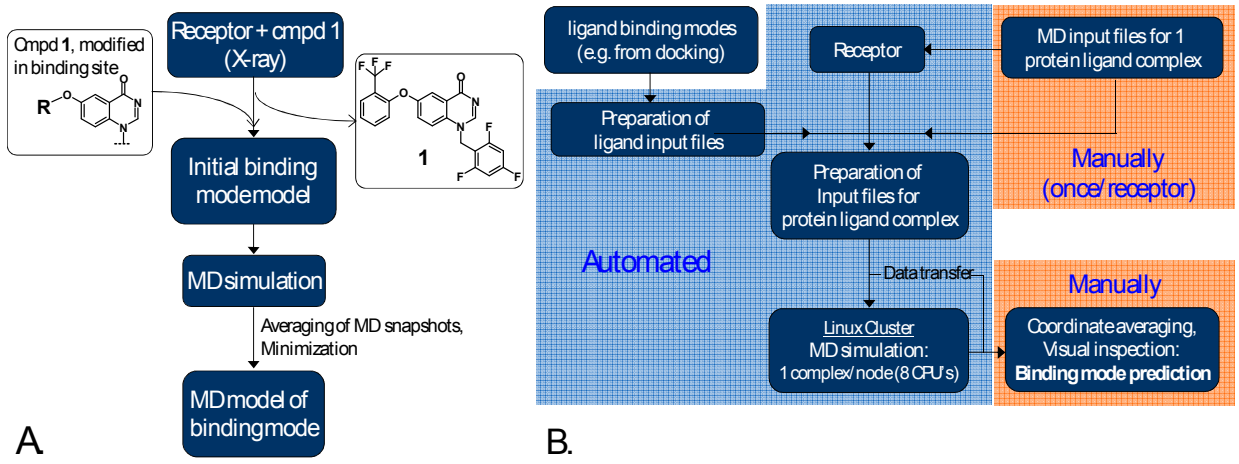

Figure 5. Graphical overview of the MD simulation protocol that was used for predicting structures of NS5B:thumb pocket 2 inhibitor complexes. **A**. General workflow for binding mode prediction of quinazolinones with LHS structure variations. **B**. Overview of the automation of the MD protocol (see Experimental section for details).

Since a hydrogen bond between the inhibitor and Leu 497 no longer appeared to be a prerequisite for the design of highly potent inhibitors, subsequent efforts shifted to capitalizing on the newly revealed interaction opportunities resulting from the ligand-induced backbone movement of the loop between Val 494 and Leu 497. The MD model of the binding mode of **6**, invoking C-H…O contacts between the pyridine ring and the carbonyl groups of Pro 495 and

Val 494, suggested that structural elements capable of forming hydrogen bonds could be beneficial. We therefore designed an indole replacement (compound **7**, Table 3) of the LHS azabenzoxazole group of **6**. Figure 6 shows the MD model for the corresponding binding mode, according to which the indole NH of **7** is located within H-bond distance (3.0 Å) from the carbonyl oxygen atoms of both Pro 495 and Val 494, with a more favorable N-H…O angle for Pro 495 (149°, as opposed to 125° for Val 494). As indicated by the superposition with the binding geometry of **6** (Fig. 6A), positions and orientations of the LHS moieties agree very well, and the indole NH occupies the position of the 6-CH group of the azabenzoxazole of **6** that is closest to the two targeted carbonyls. The side view in Figure 6B shows that the phenyl part of the indole ring partially "slips under" the displaced loop region, forming close contacts especially with Pro 496, again with the NH of Leu 497 pointing above the plane of the bicyclic ring system. The two outermost carbon atoms of the pyrrole part of the indole nucleus extend hydrophobic contacts with the bottom of the binding pocket, most importantly with the side chain of Leu 489 (not shown).

The utility of our MD prediction protocol for structure-based drug design is illustrated by the substantial 25-fold gain in cell culture antiviral potency achieved with compound **7** (Table 2) which is likely attributable to the new H-bond interaction and the described hydrophobic contacts. Indole containing inhibitor **7** is one of the most potent anti-HCV agents reported to date that acts via allosteric NS5B inhibition. The antiviral potency of **7** was tested in HCV gt1a and gt1b replicon assays, as well as gt2b, 3a, 4a, 5a, and 6a, using chimeric HCV 1b replicons that incorporate NS5B polymerase genes from these genotypes as surrogates (Table 2). The activity was in the picomolar range for the two most predominant genotypes 1a and 1b, approaching the magnitude of the exceptional potencies that were recently reported by BMS for HCV NS5A

inhibitors.[19] Notably, antiviral potency remained in the 1 – 80 nM range for all other tested NS5B genotypes, including the gt3a.

Table 2. Potency of **7** against various genotypes.

Replicon results		HCV 1b chimeric replicons with NS5B from different genotypes	
HCV genotype	EC_{50} [a] (nM)	NS5B genotype	EC_{50} [b](nM)
1a	0.12±0.02	2b	15±2
1b	0.11±0.02	3a	80±5
		4a	1.1±0.2
		5a	1.3±0.6
		6a	11±3

[a] Cell-based replicon assays with polio virus internal ribosomal entry site upstream of luciferase (see Experimental section). [b] Cross genotype cell based replicon assays.

SAR around compound **7** is summarized in Table 3 and can be rationalized using the model and aforementioned interactions with the pocket. The isomeric indole analogue **9** is predicted to be incapable of forming the corresponding hydrogen bond to Pro 495 (and Val 494). Rather, the NH is expected to point towards Arg 490 and to be solvent exposed, while polarized pyrrole C-H groups (Figure 7) are oriented towards the backbone carbonyls and extensive hydrophobic interactions are maintained with the binding site. Conversely, the MD model for compound **10**, in which the pyrrole portion of the indole system was reduced to an amino group, predicts the new H-bond to be present, but the extended hydrophobic contacts with Leu 489 are partially lost. Consistent with the predictions, compounds **9** and **10** lose approximately the same level of potency compared to **7** as they each give up one of the two main contributing factors to potency

(i.e., the new H-bond in case of **9** and part of the hydrophobic interactions in case of **10**). Compounds **13** and **14** which lack the complete pyrrole portion of the indole system and can therefore neither form favorable polar interactions with the backbone carbonyl groups of Pro 495/Val 494 nor engage in extended hydrophobic contacts with the binding site, show an additional ~ 30- to 45-fold loss in potency. Compound **11** constitutes an interesting case with a potency that is between that of the compound pairs **9/10** and **13/14**. This is rationalized by the fact that the *para*-methyl of **11** that replaces the amino group of **10** favorably extends the contact with Leu 489 and can to some degree interact favorably with the Pro 495/Val 494 carbonyls due to the positive electrostatic potential of the methyl protons pointing away from the pyridine nitrogen atom and towards the carbonyl oxygen atoms (Fig. 7). The additional methyl group in compound **12** extends hydrophobic contacts with Leu 489 compared to **10** resulting in a slight gain in potency. In the case of benzimidazole **8** on the other hand, a hydrophobic CH moiety of **7** is replaced by a hydrophilic nitrogen atom that has to be exposed to the solvent to avoid desolvation and that is unable to form optimal hydrophobic contacts with Leu 489. This may explain the observed loss in potency from 130 to 600 pM.

Table 3. SAR of compounds related to **7**

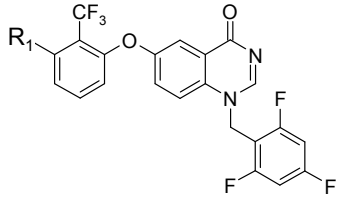

R$_1$

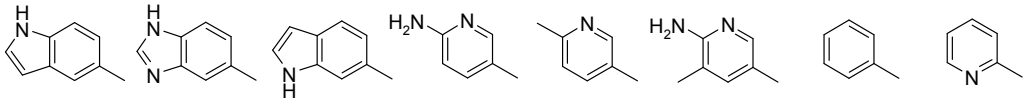

Compound	**7**	**8**	**9**	**10**	**11**	**12**	**13**	**14**
EC_{50} [a] (nM)	0.13[d]	0.6±0.2	10±6	10±2	55±4	6±2	450±92	310±45

Caco-2[b] (10^{-6} cm/s)	10.5	0.4	n.d.	4.1	n.d.	1.1	n.d.	n.d.
Sol.[c] pH2/6.8 (µg/ml)	<0.1/ <0.1	<0.1/ <0.1	<0.1/ <0.1	0.3/ <0.1	180/ <0.1	74/<0.1	n.d.	n.d.
logD(pH 7.4)	5.1	4.7	5.0	3.9	4.2	>4.7	n.d.	n.d.

[a] HCV gt 1b replicon luciferase reporter assay (n≥2).[18] [b] The Caco-2 permeability assay was run with apical pH 6.0/basolateral pH 7.4. [c] Solubility measured on lyophilized, amorphous solids using the 24 h shaking flask method. [d] n=2, identical values in both determinations

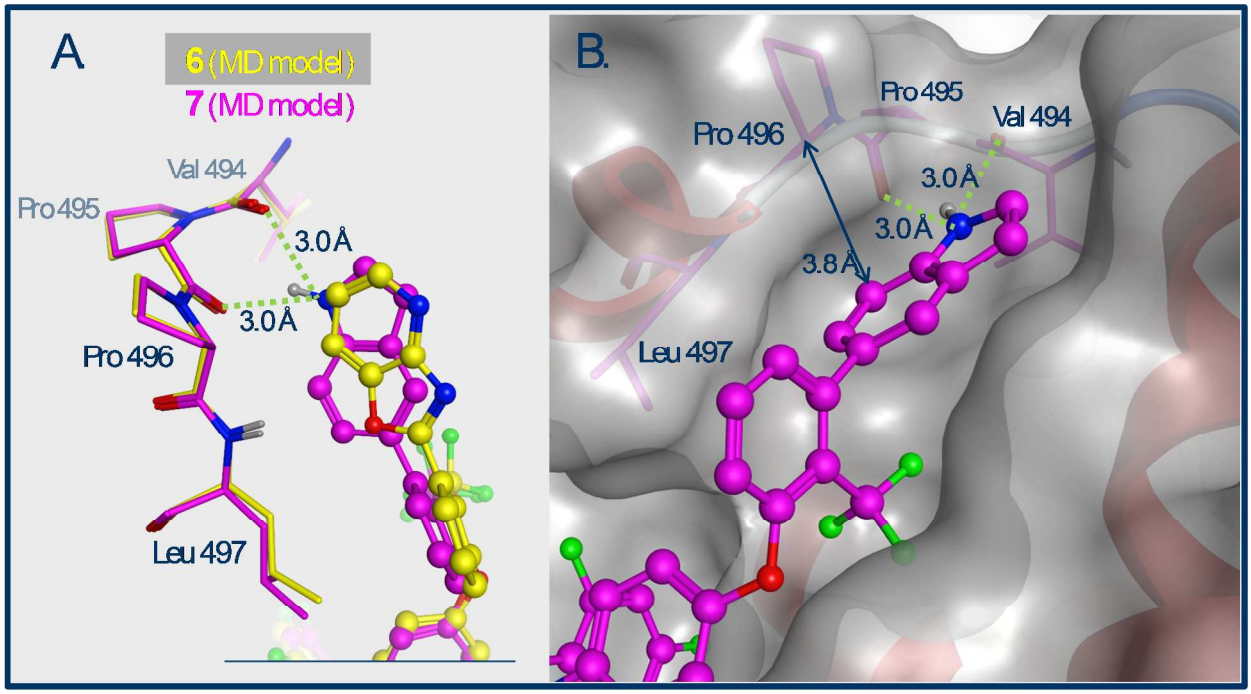

Figure 6. Binding mode of compound **7**, a picomolar thumb pocket 2 NS5B inhibitor, as predicted by the MD protocol. **A.** Superposition with the binding mode of **6**, highlighting that the NH group of the indole moiety of **7** is within H-bond distance of the backbone carbonyl groups of Pro 495 and of Val 494, replacing the favorable C-H…O contacts of **6**. Highly similar backbone conformations of the loop region between Val 494 and Leu 497 are observed with compounds **6** and **7**, i.e. both compounds lead to a similar displacement of the loop region between Val 494 and Leu 497. **B.** Surface representation of the binding pocket. The atom clash

with Pro 496 (see Fig. 3B) is avoided by the backbone movement that leads to a placement of the phenyl ring of the indole under the backbone portion of Pro 496.

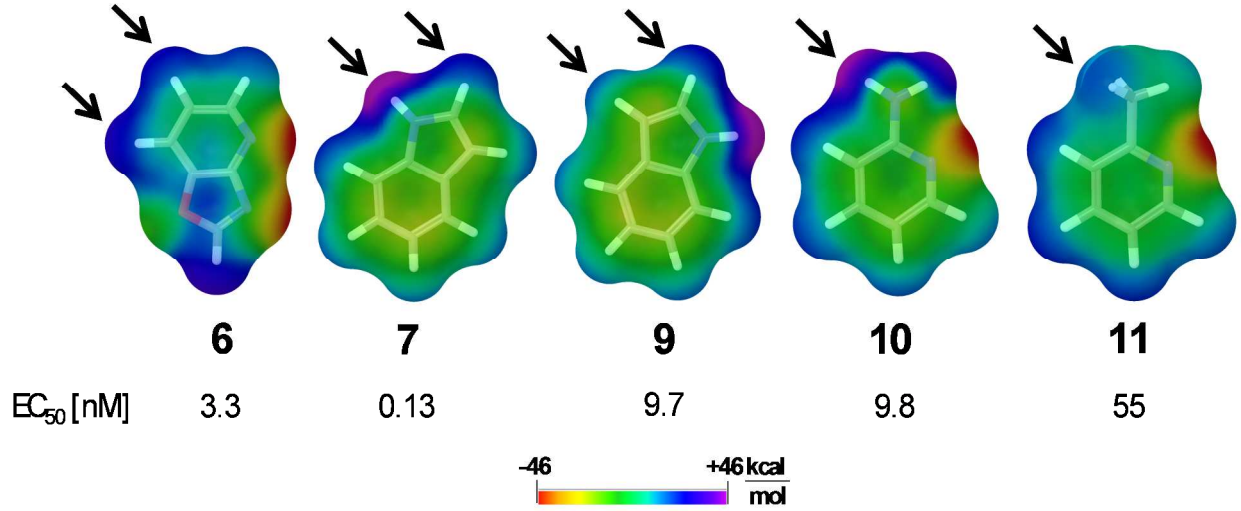

Figure 7. Computed electrostatic potential on the molecular surfaces of fragments mimicking the LHS groups of selected QAZ's (DFT at B3LYP/cc-pVTZ(-f) level, software: Jaguar, version 7.6, Schrödinger, Inc., New York, NY, 2009). Relative orientations correspond to predicted bound conformations. Arrows indicate the surface regions that are in close proximity to the (partially negative) backbone carbonyl oxygen atoms of Pro 495 and Val 494.

It is noteworthy that the picomolar inhibitor **7** displayed extremely low solubility (< 0.1 µg/mL) at pH 2 and 6.8 (Table 3). This had prompted us to explore structures with a somewhat lower molecular weight and lipophilicity. Compounds **10** and **11** reduce the molecular weight by 23 and 24 Da, respectively, and decrease the logD by approximately 1 unit lipophilicity. By keeping the new hydrogen bond to Pro 495 / Val 494, **10** manages to maintain the cell culture potency within the desirable range (< 10 nM) and shows low but measurable solubility at low pH. As a second approach to reduce lipophilicity and molecular weight, we explored QAZs lacking the *ortho*-trifluoromethyl group of the LHS phenyl ring but taking advantage of the

newly discovered interactions with Pro 495/Val 494 (*des*-CF_3 compounds; Table 4). Prior to synthesis, the potential of this strategy was evaluated through MD simulations. The results clearly suggested that in order to reach the beneficial interactions with Pro 495/Val 494 the point of substitution had to be moved from the *meta* to the *para* position (Figure 8): in absence of the CF_3 group, the position of the phenyl ring shifts in the binding pocket towards the vacated "CF_3-pocket" in order to occupy the available space (Figure 8B) – for the *des*-CF_3 phenyl ring the corresponding conformation relative to the QAZ core is in good agreement with the low energy conformation in solution. However, it is noteworthy that the phenyl ring cannot fill the "CF_3 pocket" in an optimal fashion, due to inadequate shape complementarity with the narrow hydrophobic depression in the TP-2 surface that is surrounded by the side chains of Leu 419, Met 423 and Val 485 and that was optimally filled by the CF_3 moiety. A drop in potency is therefore expected, even if all the other interactions were maintained. This was in agreement with previous SAR work that showed that omitting the CF_3 group leads to a systematic ~ 10-fold loss in potency (data not shown). Another contributing factor to this loss in activity could be that *des*-CF_3 compounds are expected to pay a higher entropic cost upon binding to NS5B, as the presence of the relatively bulky *ortho*-CF_3 group limits the conformational space that is accessible to the LHS phenyl moiety. For all these reasons, it was not surprising to see a substantial loss in potency for compound **15** that shares the azabenzoxazole group of CF3-containing analogue **6**. However, it was gratifying that the loss in potency can be partially compensated by using the LHS indole group of **7**. Compound **16**, which is predicted to form a hydrogen bond with the carbonyl of Pro 495 (Figure 8) had EC_{50} = 4.6 nM. This result highlights that carefully designed *des*-CF_3 molecules that make use of the newly discovered H-bond interaction, can still achieve low nM potency. **16** is an example of a potent QAZ inhibitor with

reduced molecular weight (498 Da compared to 566 Da for **7**) and decreased lipophilicity (logD = 4.4 *vs* 5.1). Unfortunately this did not translate into substantially improved solubility, and the *des*-CF_3 series was not further pursued.

Table 4 Examples of two *des*-CF_3 compounds. **15** and **16** use the LHS extensions of **6** and **7**, attached to the phenyl ring in the para position based on modeling results.

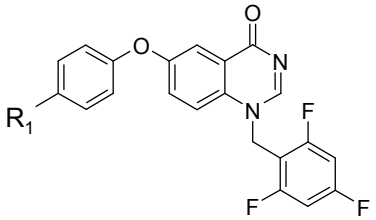

R_1

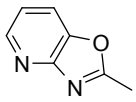

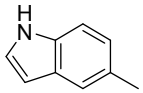

Compound	**15**	**16**
EC_{50} [a] (nM)	490±140	4.6±2.4
CACO-2[b] (10^{-6} cm/s)	n.d.	3.5
Sol.[c] pH 2/6.8 (µg/ml)	n.d.	<0.1/0.18
logD(pH 7.4)	n.d.	4.4

[a] HCV gt 1b replicon luciferase reporter assay (n≥2).[18] [b] The Caco-2 permeability assay was run with apical pH 6.0/basolateral pH 7.4. [c] Solubility measured on lyophilized, amorphous solids using the 24 h shaking flask method.

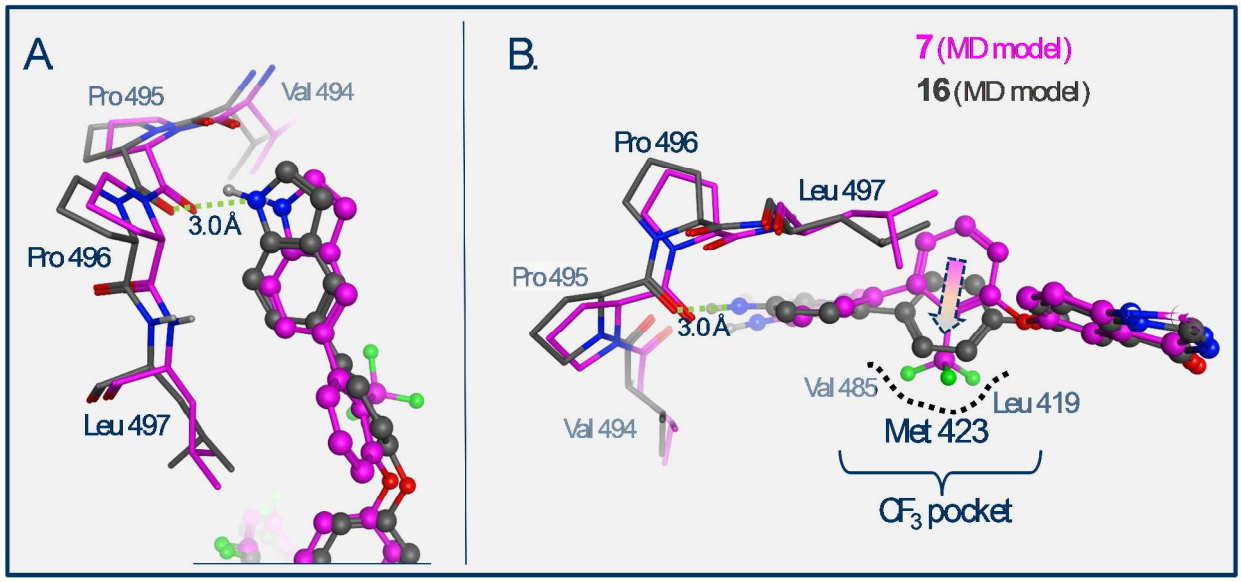

Figure 8. Superposition of MD models for *des*-CF_3 compound **16** and compound **7**. **A.** Both show similar positions of the indole moiety and are predicted to form a H-bond to Pro 495. **B.** The side view shows the repositioning of the LHS phenyl ring of **16** relative to **7** as a consequence of the absence of the CF_3 group, requiring the attachment of the indole in the para instead of the meta position for *des*-CF_3 compounds (only the QAZ core and the LHS part are shown, for clarity). The small pocket that is occupied by the CF_3 group is shown as a dotted line, the surrounding amino acids are indicated.

CHEMISTRY

The N^1-2,4,5-triflurobenzylquinazolinone scaffold was built from 5-hydroxy-2-aminobenzoic acid **17** as shown in Scheme 1. A reductive amination was used to introduce the 2,4,5-triflurobenzyl group onto **17**. The quinazolinone heterocycle **19** was formed by refluxing **18** with formamidine acetate in 2-methoxyethanol. Hydroxylquinazolinone **19** could not be directly coupled with methyl-3-fluoro-2-trifluoromethylbenzoate to form biarylether **23** without concomitant decomposition. The problem was circumvented by first reducing **19** to hydroxyquinazolidinone **20** thereby making the phenolic oxygen more nucleophilic. This

allowed SN_{AR} coupling to proceed at a lower temperature and **22** could be recovered in acceptable yield. Saponification followed by oxidation afforded acid intermediate **23** that was coupled with the appropriate amines to afford inhibitors **2**-**5**.

Scheme 1. Synthesis of carboxamide inhibitors **2**- **5**.

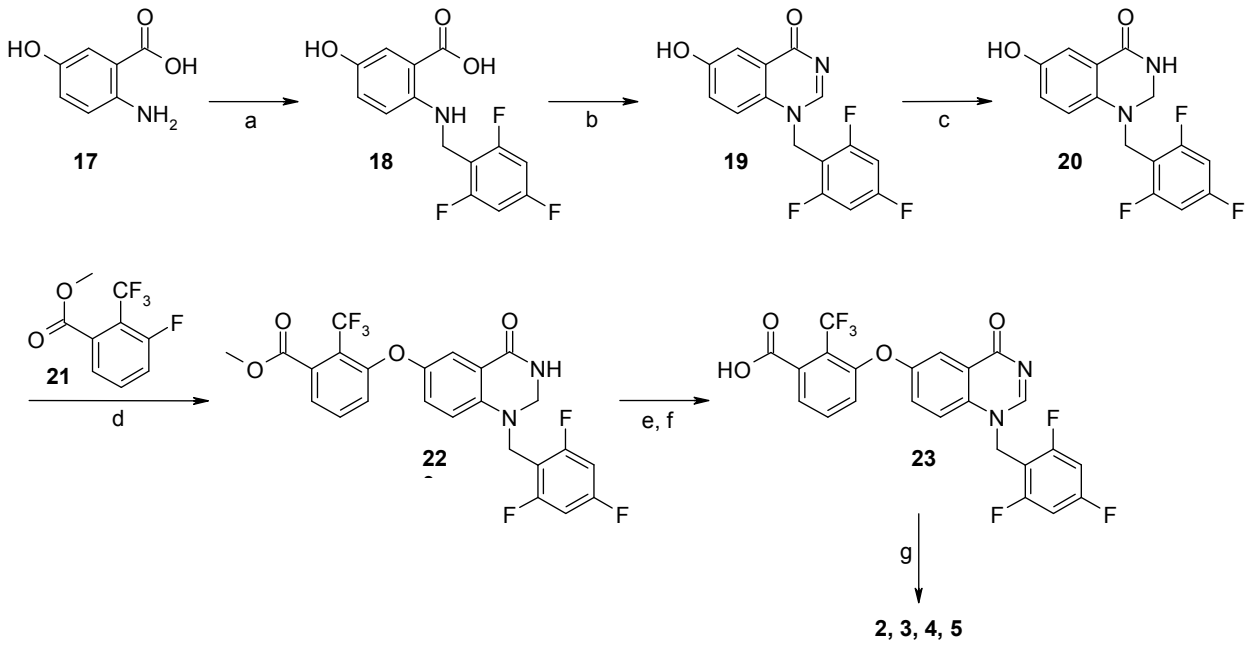

(a) 2,4,6-trifluorobenzaldehyde, $NaCNBH_3$, AcOH, 0 ^oC to RT, 16 h; (b) formamidine acetate, 2-methoxyethanol, reflux, 4 h; (c) $NaBH_4$, MeOH, RT, 16 h; (d) **20**, Cs_2CO_3, DMF, 50 ^oC, 24 h; (e) NaOH, MeOH/THF, RT, 4 d; (f) I_2, Na_2CO_3, MeOH, RT, 3 h; (g) NH_3 or aniline or aminopyridine, HATU, NEt_3, DMF, RT, 3 h

Aryl substituted inhibitors **6-16** were prepared as shown in Scheme 2. Hydroxyquinazolinone **19** was found to couple efficiently with 2-bromo-6-fluorobenzotrifluoride **24** to form **25** without the reduction/oxidation sequence required to prepare **23**. Direct arylation of **25** with 4-azabenzoxazole to synthesize **6** was achieved using conditions adapted from the literature[20].

Suzuki-Miyaura cross-couplings were used to prepare inhibitors **7**, **10-13** and pyridine-substituted inhibitor **14** was obtained from a Stille cross-coupling. Alternatively, bromide **25** could be borylated with bis(pinacolato)diboron[21] to provide boronic ester **26**, that was subsequently cross-coupled with 6-bromoindole to afford inhibitor **9**. Linear inhibitors **15** and **16** were prepared from iodide **27** using similar protocols.

Scheme 2. Synthesis of aryl substituted inhibitors **6-16**.

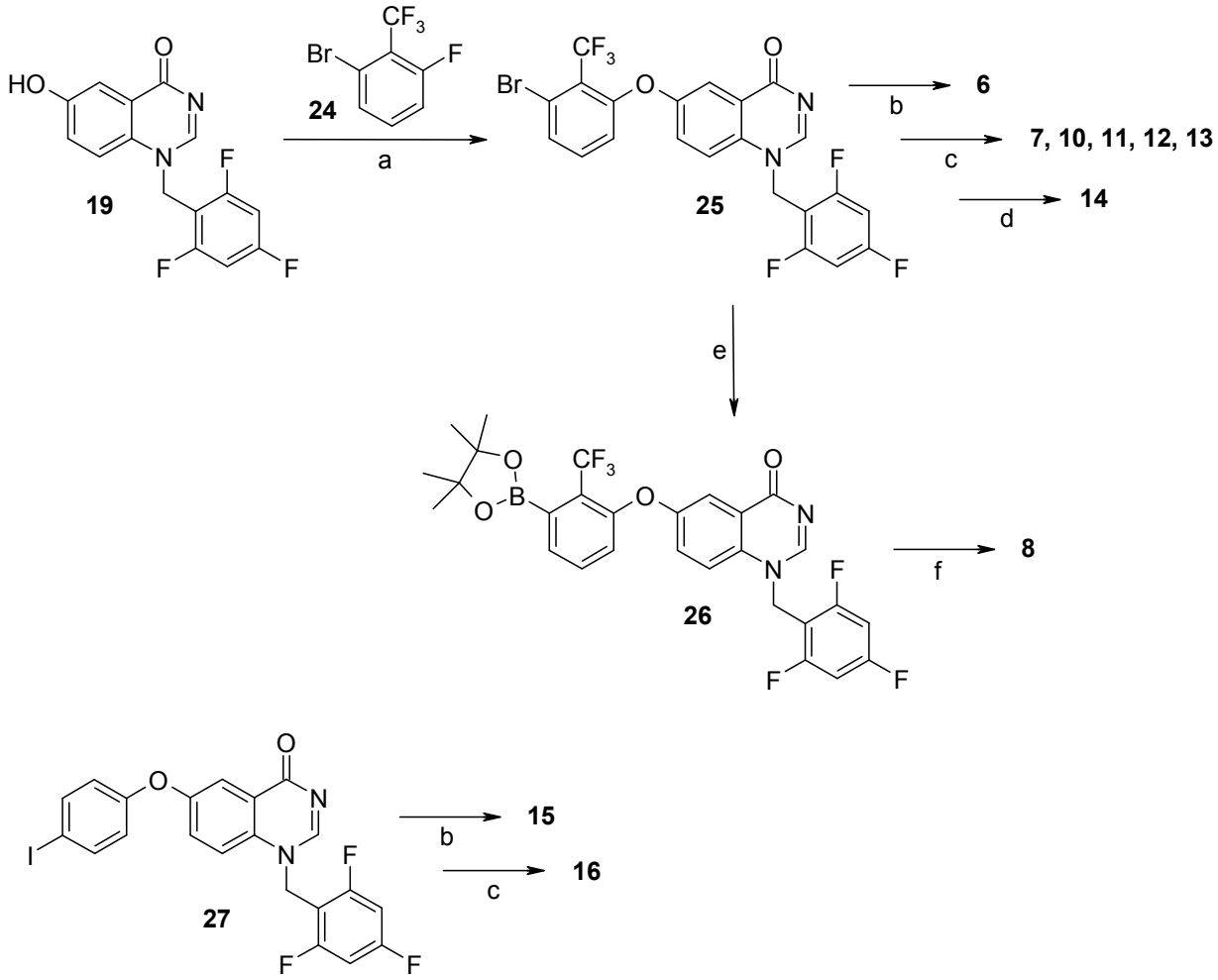

(a) **23**, Cs_2CO_3, DMF, 40 °C, 3 d; (b) 4-azabenzoxazole, KOAc, TBAB, CuI, (t-$Bu_3P)_2Pd$, DMF, 170 °C, 10 min.; (c) boronic acid, aq. Na_2CO_3, $(Ph_3P)_4Pd$, DMF, 170 °C, 10 min.; (d) 2-

(tributylstannyl)pyridine, $(Ph_3P)_4Pd$, DMF, 80 ^oC, 18 h; (e) bis(pinacolato)diboron, KOAc, $(dppf)PdCl_2$, DMF, 95 ^oC, 9 h; (f) 6-bromoindole, aq. Na_2CO_3, $(Ph_3P)_4Pd$, DMF, 120 ^oC, 15 min.

CONCLUSION

Substantial gains in potency were realized in the quinazolinone series of NS5B thumb pocket 2 allosteric inhibitors by extending into the left hand side of the binding pocket, towards residues Pro 495 and Val 494. A structure-based design approach was successfully applied for this purpose. However, the use of established crystallographic protocols was limited due to ligand induced crystal cracking. A molecular dynamics based structure prediction workflow was therefore established and used as the main tool to support optimization efforts. This method predicted a shift of the protein backbone in the loop region between Val 494 and Leu 497, somewhat enlarging the pocket and, most importantly, improving accessibility of the backbone carbonyl groups of Pro 495 and Val 494. The design of a structure with the capacity to form H-bonds with these acceptor groups yielded an inhibitor with picomolar potency against the most prevalent HCV genotypes (gt1a EC_{50} = 120 pM and gt 1b EC_{50} = 110 pM) and double digit nanomolar activity against genotypes 2-6, inclusively. Compound **7** is one of the most potent *anti*-HCV agents known to date that acts via allosteric NS5B inhibition. The high level of antiviral activity provides significant leeway to balance potency with ADMET-PK properties such as solubility-limited oral exposure. The identification of QAZ analogs with improved overall profiles and potential for further development will be the subject of future reports. The success of the structure based design efforts guided by the MD predictions underlines that the MD workflow may be used in a broader fashion as a general protocol for modeling the interactions of NS5B with diverse thumb pocket 2 ligands.

EXPERIMENTAL SECTION

X-ray crystallography

X-ray crystal structures of NS5B inhibitor complexes were obtained by soaking preformed *apo* NS5B crystals into a solution of inhibitor (1mM). For some of the inhibitors of pocket 2, it was found that the diffraction resolution diminished proportionally to the soaking time. Successful co-structure data were obtained by adjusting the time of soaking such that sufficient pocket 2 inhibitor occupancy occurred without leading to unusable crystals due to cracking. Adjustments were made through trial-and-error by varying crystal size, soaking time and compound concentration. For example, the structure of compound **6** was obtained by reducing the soaking time to 3 hours and the concentration to 0.5 mM. Longer soaking time lead to loss of diffraction, shorter soaking time resulted in low occupancy and poor inhibitor electron density maps.

Crystals of *apo* NS5B polymerase were obtained using the hanging drop technique with a Nextal plate (Qiagen). The protein was prepared from constructs of HCV NS5B 1bJ4 strain that lack the C-terminal 21 amino acids and encode for a C-terminal hexa-histidine tag.[22] The protein was purifed as previously described[23] and concentrated to 8.6 mg/ml in a buffer containing 25 mM tris at pH 7.5, 300 mM NaCl, 10% glycerol and 2 mM TCEP. The crystallization solution used was made of 21% PEG 5000 mme, 100 mM MES pH 5.4, 10% glycerol and 410 mM ammonium sulfate. Hanging drops of 2 µl were incubated at 11 ˚C and crystals were grown within 5 days. For soaking experiments, single crystals were transferred to a solution made of 14% PEG 5000 mme, 74 mM tris pH 7,5, 500 mM NaCl, 14% glycerol, 1% PEG 20K and 1 mM of compounds.

Diffraction data were collected at the Swiss Light Source (SLS) PX1 beamline or locally on a Rigaku FRE generator equipped with a MAR345 detector. The structures were solved by

molecular replacement using our published *apo* structure (3MWV), Model refinement was performed using the CNX software (Accelrys). The NS5B co-structures with compound **1**, **2**, **4**, **6** and **14** have been deposited in the Protein Data Bank (accession codes 4JTW, 4JTY, 4JTZ, 4JU1 and 4JU2 respectively).

Structure prediction of NS5B:ligand complexes using molecular dynamics simulations

The X-ray structure with compound **1** served as starting point for the preparation of the receptor coordinates for MD simulations. To limit the number of atoms and computational cost, only the thumb domain (S365-S563) and part of the finger loop (S19-A39) were considered. Harmonic restraints (50 kcal/mol) were applied to residues that are involved in interactions with the deleted protein parts, to mimic the dampening effect of these contacts on the flexibility of this set of interface residues (38 of a total of 220 considered residues, i.e. 83% of the protein were fully flexible in the simulations). The restrained residue closest to compound **1** was located at a distance of 13 Å, confirming that the binding pocket and its surroundings were fully flexible. In order to focus the sampling of the simulations on the LHS region of the ligand structure, harmonic distance restraints (1 kcal/mol) were introduced to favor the conserved H-bond interactions in the RHS region between the quinazolinone core and the backbone NH groups of Ser 476 and Tyr 477.

In summary, the MD simulation protocol comprisedthe following steps: 1. Minimization, first with strong restraints (50 kcal/mol) on the solute (protein ligand complex) which were successively released in 3 minimization cycles (last cycle without restraints on non-interface residues); 2. Equilibration in 3 steps, with an overall simulation time of 250 ps: a.) slow heating to the simulation temperature of 298 K (harmonic restraints of 5 kcal/mol on non-interface

residues, 50 ps), b.) pressure adjustment to 1 atm (harmonic restraints of 1 kcal/mol on non-interface residues, 100 ps), c.) final NVT equilibration (no restraints on non-interface residues, 100 ps); 3. Production: NPT simulation, simulation time = 1.25 ns, no restraints on non-interface residues (total simulation time = 1.5 ns). AMBER8 [24] was used for all simulations, employing the ff03 force field,[25] AM1BCC charges[26] for the ligand in combination with the gaff force field.[27] Water was considered explicitly (TIP3P model), using a truncated octahedron solvent box with the distance from the box surface to the closest solute atoms set to 12 Å. The overall protein charge was neutralized by introducing amino acid changes in solvent exposed areas distant from the ligand binding site (K20D, K379D, R394A, K441D, R465A, K510D, K535D). This approach was chosen to avoid extended equilibration times that are often needed for the proper configurational sampling of ions.

Starting models for new ligands were obtained by modification of **1** and minimization within the binding site, using MOE. Resulting binding mode hypotheses were exported as mol2 files and submitted to a semi-automatic structure prediction protocol (Figure 5): Ligand coordinates from a mol2 file were automatically combined with the receptor coordinates. The corresponding pdb file was the basis for generating the AMBER input files, which were transferred to our Linux cluster. There, the MD simulation for each protein ligand complex was conducted on 8 cores of one computing node in parallel using sander. Upon completion, the output data was transferred back to the workstation of the computational chemist. This process was automated through a Perl program. Output trajectories were visually inspected, along with the rmsd trace of the ligand coordinates, to identify distinct relevant binding poses that were sampled in the simulation. The corresponding coordinate sets of the trajectory were averaged, and the average was minimized to obtain the final predicted MD binding mode model. The simulation of one

protein ligand complex took approximately 10 hours and was usually done overnight, allowing for an overall turnaround time of ~ 24 hours for setting up a simulation, running it, doing the analysis and providing the results to the medicinal chemistry team.

The MD structure prediction protocol was validated prior to its application in the project by applying it to compound **4**, for which an X-ray structure existed. As described above, compound **1** (in its corresponding X-ray structure) was modified to compound **4** and the resulting initial model of the binding mode was submitted to the MD protocol. In the resulting MD model, the rmsd from the X-ray structure amounted to 0.8 Å (ligand coordinates, non-hydrogen atoms; see supporting information for a figure of the superposition of MD model and X-ray structure). These validation results and the successful predictive application of the established MD protocol in the project suggest that it can be used as a general modeling approach for the interaction of NS5B with thumb pocket 2 inhibitors, under consideration of protein flexibility.

HCV replicon cell based assays.

Cell culture EC_{50} potency and inhibition of HCV RNA replication with HCV subgenomic 1b and 1a replicons were assessed as previously described using the cell-based 1b luciferase reporter assay or replicon assays using RT-PCR for RNA quantification.[18]

Additional replicon assays used HCV subgenomic luciferase reporter replicons that incorporated the polio virus internal ribosomal entry site upstream of luciferase, increased assay sensitivity and provided EC_{50} for reference compounds that were consistent with the previously established luciferase reporter replicon results.

Potencies for non-1 genotype were determined by the use of chimeric gt1b sub genomic replicons that substituted the endogenous NS5B with those from other genotypes. Briefly, the

entire NS5B portion obtained from patient samples of the listed genotypes (2b, 3a, 4a, 5a and 6a) was introduced into a bicistronic gt1b NS5B shuttle vector. The shuttle vector (p712) featured a luciferase reporter gene in the first cistron that was preceded by the HCV 5'UTR, whereas the second cistron encoded the NS2 to NS5B portion of the HCV non-structural proteins, the HCV 3'UTR and 3 copies of the HDV ribozyme. *In vitro* synthesized replicon RNA for each replicon or chimeric replicon was introduced into HuH7-J cells by electroporation to generate stable cell lines. These cell lines were then exposed for 72 hours to various serial dilutions of polymerase inhibitors or control drugs (interferon alpha or protease inhibitors). The potency and half maximal effect at inhibiting HCV RNA replication was assessed by measuring the luciferase levels or the number of copies of replicon RNA by real-time PCR in the case of the genotype 6a chimera.

ASSOCIATED CONTENT

Supporting Information Available.

^{1}H NMR spectra for inhibitors **1-7**, **9-11**, **13-16**; ^{13}C NMR spectra for compounds **1**, **3-5**, **7, 9-11, 13-16**; ^{19}F NMR spectra for compounds **1**, **2**, **14-16**; HRMS data for cpds **1**, **3-5**, **7, 9-11, 13-16**; Additional details on the setup of the NS5B protein for MD simulations; Validation of the simulation protocol through application to compound **4.** This material is available free of charge via the Internet at http://pubs.acs.org.

Corresponding Author

*Dr. Oliver Hucke, oliver.hucke@boehringer-ingelheim.com; ++49 7351 / 54-99462

PDB ID Codes: 4JTW, 4JTY, 4JTZ, 4JU1, 4JU2

Acknowledgement

We thank the following colleagues from Boehringer Ingelheim (Canada) Ltd. who participated in generating the data presented in this paper: Nathalie Dansereau, Lisette Lagacée for EC_{50} determinations; Norman Aubry, Sylvain Bordeleau, Colette Boucher for analytical support; A. Jakalian for helpful discussions of MD simulations.

Abbreviations Used

MD, Molecular Dynamics; QAZ, quinazolinone; HCV, hepatitis C virus; DAA, direct acting antiviral; PegIFN, pegylated interferon; IFN, interferon; RBV, ribavirin; gt1, genotype 1; SVR, sustained viral response; SoC, standard of care; RdRp, RNA-dependent RNA polymerase; TP-1, thumb pocket 1; ESP, electrostatic surface potential; ADME, absorption, distribution, metabolism, excretion; PK, pharmacokinetics; rmsd, root mean square deviation; SAR, structure−activity relationship; THF, tetrahydrofuran; DMF, N,N-dimethylformamide; HATU, O-(7-azabenzotriazol-1-yl)-N,N,N’,N’-tetramethyluronium hexafluorophosphate

REFERENCES

1. Lavanchy, D. Evolving epidemiology of hepatitis C virus. *Clin. Microbiol. Infect.* **2011**, *17*, 107-115.

2. (a) Bosetti, C.; Levi, F.; Lucchini, F.; Zatonski, W. A.; Negri, E.; La, V. C. Worldwide mortality from cirrhosis: an update to 2002. *J. Hepatol.* **2007**, *46*, 827-839. (b) Wise, M.; Bialek, S.; Finelli, L.; Bell, B. P.; Sorvillo, F. Changing trends in hepatitis C-related mortality in the United States, 1995-2004. *Hepatology* **2008**, *47*, 1128-1135. (c) Davila, J. A.;

Morgan, R. O.; Shaib, Y.; McGlynn, K. A.; El-Serag, H. B. Hepatitis C infection and the increasing incidence of hepatocellular carcinoma: a population-based study. *Gastroenterology* **2004**, *127*, 1372-1380.

3. (a) National Institutes of Health consensus development conference statement: management of hepatitis C 2002 (June 10−12, 2002). *Gastroenterology* **2002**, *123*, 2082−2099. (b) Manns, M. P.; Foster, G. R.; Rockstroh, J. K.; Zeuzem, S.; Zoulim, F.; Houghton, M. The way forward in HCV treatment: finding the right path. *Nat. Rev. Drug Discovery* **2007**, *6*, 991−1000. (c) Björnsson, E.; Verbaan, H.; Oksanen, A.; Frydén, A.; Johansson, J.; Friberg, S.; Dalgård, O.; Kalaitzakis, E. Health-related quality of life in patients with different stages of liver disease induced by hepatitis C. *Scand. J. Gastroenterol.* **2009**, *44*, 878−887.

4. (a) Hinrichsen, H.; Benhamou, Y.; Wedemeyer, H.; Reiser, M.; Sentjens, R. E.; Calleja, J. L.; Forns, X.; Erhardt, A.; Cronlein, J.; Chaves, R. L.; Yong, C. L.; Nehmiz, G.; Steinmann, G. G. Short-term antiviral efficacy of BILN 2061, a hepatitis C virus serine protease inhibitor, in hepatitis C genotype 1 patients. *Gastroenterology* **2004**, *127*, 1347-1355. (b) Lamarre, D.; Anderson, P. C.; Bailey, M.; Beaulieu, P.; Bolger, G.; Bonneau, P.; Bos, M.; Cameron, D. R.; Cartier, M.; Cordingley, M. G.; Faucher, A. M.; Goudreau, N.; Kawai, S. H.; Kukolj, G.; Lagace, L.; LaPlante, S. R.; Narjes, H.; Poupart, M. A.; Rancourt, J.; Sentjens, R. E.; St, G. R.; Simoneau, B.; Steinmann, G.; Thibeault, D.; Tsantrizos, Y. S.; Weldon, S. M.; Yong, C. L.; Llinas-Brunet, M. An NS3 protease inhibitor with antiviral effects in humans infected with hepatitis C virus. *Nature* **2003**, *426*, 186-189.

5. Berman, K.; Kwo, P. Y. Boceprevir, an NS3 protease inhibitor of HCV. *Clin. Liver Dis.* **2009**, *13*, 429-439.

6. (a) Gentile, I.; Carleo, M. A.; Borgia, F.; Castaldo, G.; Borgia, G. The efficacy and safety of telaprevir - a new protease inhibitor against hepatitis C virus. *Expert. Opin. Investig. Drugs* **2010**, *19*, 151-159. (b) Kwong, A. D.; Kauffman, R. S.; Hurter, P.; Mueller, P. Discovery and development of telaprevir: an NS3-4A protease inhibitor for treating genotype 1 chronic hepatitis C virus. *Nat. Biotechnol.* **2011**, *29*, 993-1003.

7. Asselah, T.; Marcellin, P. New direct-acting antivirals' combination for the treatment of chronic hepatitis C. *Liver Int.* **2011**, *31* Suppl 1, 68-77.

8. (a) Tanwar, S.; Trembling, P. M.; Dusheiko, G. M. TMC435 for the treatment of chronic hepatitis C. *Expert. Opin. Investig. Drugs* **2012,** *21*, 1193-1209. (b) Lenz, O.; Vijgen, L.; Berke, J. M.; Cummings, M. D.; Fevery, B.; Peeters, M.; Smedt, G. D.; Moreno, C.; Picchio, G. Virologic response and characterization of HCV genotype 2-6 in patients receiving TMC435 monotherapy (study TMC435-C202). *J. Hepatol.* **2013,** *58*, 445-451

9. (a) White, P. W.; Llinas-Brunet, M.; Amad, M.; Bethell, R. C.; Bolger, G.; Cordingley, M. G.; Duan, J.; Garneau, M.; Lagace, L.; Thibeault, D.; Kukolj, G. Preclinical characterization of BI 201335, a C-terminal carboxylic acid inhibitor of the hepatitis C virus NS3-NS4A protease. *Antimicrob. Agents Chemother.* **2010**, *54*, 4611-4618. (b) Lemke, C. T.; Goudreau, N.; Zhao, S.; Hucke, O.; Thibeault, D.; Llinas-Brunet, M.; White, P. W. Combined X-ray, NMR, and kinetic analyses reveal uncommon binding characteristics of the hepatitis C virus NS3-NS4A protease inhibitor BI 201335. *J. Biol. Chem.* **2011**, *286*, 11434-11443.

10. Poordad, F.; Cohen, D. E.; Nelson, D. R.; Zeuzem, S.; Everson, G. T.; Kwo, P. Y.; Foster, G. R.; Sulkowski, M. S.; Xie, W.; Pilot-Matias, T.; Liossis, G.; Larsen, L. M.; Khatri, A.; Podsadecki, T. J.; Bernstein, B. Exploratory study of oral combination antiviral therapy for

hepatitis C. Presented at the 63rd Annual Meeting of the American Association for the Study of the Liver Diseases (AASLD) November 9 – 13th, Boston, MA, late-braker abstract LB-1; *N. Engl. J. Med.* **2013**, *368*, 45-53.

11. (a) Zeuzem, S.; Asselah, T.; Angus, P.; Zarski, J.-P.; Larrey, D.; Müllhaupt, B.; Gane, E.; Schuchmann, M.; Lohse, A.; Pol, S.; Bronowicki, J.-P.; Roberts, S.; Arasteh, K.; Zoulim, F.; Heim, M.; Stern, J. O.; Kukolj, G.; Nehmiz, G.; Haefner, C.; Boecher, W. O. Efficacy of the protease inhibitor BI 201335, polymerase inhibitor BI 207127, and ribavirin in patients with chronic HCV infection. *Gastroenterology* **2011**, *141*, 2047. (b) Zeuzem, S.; Gane, E.; Roberts, S.; Mensa, F. *J. Gastroent. Hepatol.* **2012**, *27* (Suppl. 4), 182.

12. The X-ray structure of HCV NS5B and the role of the structural domains were first described in: (a) Ago, H.; Adachi, T.; Yoshida, A.; Yamamoto, M.; Habuka, N.; Yatsunami, K.; Miyano, M.: Crystal structure of the RNA-dependent RNA polymerase of hepatitis C virus. *Structure* **1999**, *7*, 1417-1426. (b) Bressanelli, S.; Tomei, L.; Roussel, A.; Incitti, I.; Vitale, R. L.; Mathieu, M.; De Francesco, R.; Rey, F. A. Crystal structure of the RNA-dependent RNA polymerase of hepatitis C virus. *Proc. Natl. Acad. Sci. USA* **1999**, *96*, 13034-13039.

13. TP-2 was initially revealed by Agouron, with a dihydropyrone ligand bound: (a) Love, R. A.;Yu, X.; Diehl, W.; Hickey, M. J.; Parge, H. E.; Gao, J.; Fuhrman, S. *Patent* EP 12566628, **2002**. (b) Love, R. A.; Parge, H. E.; Yu, X.; Hickey, M. J.; Diehl, W.; Gao, J.; Wriggers, H.; Ekker, A.; Wang, L.; Thomson, J. A.; Dragovich, P. S.; Fuhrman, S. A. Crystallographic identification of a noncompetitive inhibitor binding site on the hepatitis C virus NS5B RNA polymerase enzyme. *J. Virol.* **2003**, *77*, 7575.; Shire Biochem described the crystal structure of a different chemotype bound to TP-2: (c) Wang, M.; Ng, K. K.; Cherney, M. M.;

Chan, L.; Yannopoulos, C. G.; Bedard, J.; Morin, N.; Nguyen-Ba, N.; Alaoui-Ismaili, M. H.; Bethell, R. C.; James, M. N. Non-nucleoside analogue inhibitors bind to an allosteric site on HCV NS5B polymerase. Crystal structures and mechanism of inhibition. *J. Biol. Chem.* **2003,** *278*, 9489-9495.

14. For recent reviews on allosteric NS5B inhibition see: (a) Beaulieu, P. L. Recent advances in the development of NS5B polymerase inhibitors for the treatment of hepatitis C virus infection. *Expert. Opin. Ther. Pat* **2009,** *19*, 145-164. (b) Haudecoeur, R.; Peuchmaur, M.; Ahmed-Belkacem, A.; Pawlotsky, J. M.; Boumendjel, A. Structure-Activity Relationships in the Development of Allosteric Hepatitis C Virus RNA-Dependent RNA Polymerase Inhibitors: Ten Years of Research. *Med. Res. Rev.* **2012**. (c) P. L. Beaulieu in "Successful Strategies for the Discovery of Antiviral Drugs" M. C. Desai and N. A. Meanwell Editors, RSC Publishing, Cambridge, UK, **2013** (in press).

15. Stammers, T. A.; Coulombe, R.; Rancourt, J.; Thavonekham, B.; Fazal, G.; Goulet, S.; Jakalian, A.; Wernic, D.; Tsantrizos, Y.; Poupart, M.-A.; Bös, M.; McKercher, G.; Thauvette, L.; Kukolj, G.; Beaulieu, P. L.; Discovery of a Novel Series of Non-Nucleoside Thumb Pocket 2 HCV NS5B Polymerase Inhibitors (submitted).

16. Beaulieu, P. L.; Coulombe, R.; Duan, J.; Fazal, G.; Godbout, C.; Hucke, O.; Jakalian, A.; Joly, M.-A.; Lepage, O.; Llinàs-Brunet, M.; Naud, J.; Poirier, M.; Rioux, N.; Thavonekham, B.; Kukolj, G.; Timothy A. Stammers. Structure-Based Design of Novel HCV NS5B Thumb Pocket 2 Allosteric Inhibitors with Submicromolar gt1 Replicon Potency: Discovery of a Quinazolinone Chemotype. *Bioorg. Med. Chem. Lett.*, **2013**, *23*, DOI:10.1016/j.bmcl.2013.05.037.

17. Note: Solubility limitations in the biochemical assay buffer led to undiscriminating SAR for some compounds and therefore, cell-based antiviral potencies (EC_{50}) are used throughout for interpretation of the data.

18. (a) Beaulieu, P. L.; Fazal, G.; Goulet, S.; Kukolj, G.; Poirier, M. ; Tsantrizos, Y. ; Jolicoeur, E. ; Gillard, J. ; Poupart, M. –A.; Rancourt, J. WO Patent WO 03/010141, 2003. (b) Llinàs-Brunet, M.; Bailey, M. D.; Goudreau, N.; Bhardwaj, P. K.; Bordeleau, J.; Bös, M.; Bousquet, Y.; Cordingely, M. G.; Duan, J.; Forgione, P.; Garneau, M.; Ghiro, E.; Gorys, V.; Goulet, S.; Halmos, T.; Kawai, S. H.; Naud, J.; Poupart, M. –A.; White, P. W. *J. Med. Chem.* **2010**, *53*, 6466-6476. (c) Vaillancourt, F. H.; Pilote, L.; Cartier, M.; Lippens, J.; Liuzzi, M.; Bethell, R. C.; Cordingley, M. G.; Kukolj, G. *Virology* **2009**, *387*, 5-10.

19. (a) Gao, M.; Nettles, R. E.; Belema, M.; Snyder, L. B.; Nguyen, V. N.; Fridell, R. A.; Serrano-Wu, M. H.; Langley, D. R.; Sun, J. H.; O'Boyle, D. R.; Lemm, J. A.; Wang, C.; Knipe, J. O.; Chien, C.; Colonno, R. J.; Grasela, D. M.; Meanwell, N. A.; Hamann, L. G. Chemical genetics strategy identifies an HCV NS5A inhibitor with a potent clinical effect. *Nature* **2010,** *465*, 96-100. (b) Belda, O.; Targett-Adams, P. Small molecule inhibitors of the hepatitis C virus-encoded NS5A protein. *Virus Res.* **2012,** *170*, 1-14.

20. (a) McClure, M. S.; Glover, B.; McSorley, E.; Millar, A.; Osterhout, M. H.; Roschangar, F. Regioselective Palladium-Catalyzed Arylation of 2-Furaldehyde. *Org. Lett.* **2001**, *3*, 1677-1680. (b) Pivsa-Art, S.; Satoh, T.; Kawamura, Y.; Miura, M.; Nomura, M. Palladium-Catalyzed Arylation of Azole Compounds with Aryl Halides in the Presence of Alkali Metal Carbonates and the Use of Copper Iodide in the Reaction. *Bull. Che. Soc. Jpn.* **1998**, *71*, 467-473.

21. Ishiyama, T.; Murata, M.; Miyaura, N. Palladium(0)-catalyzed cross-coupling reaction of alkoxydiboron with haloarenes: A direct procedure for arylboronic esters. *J. Org. Chem.* **1995**, *60*, 7508-7510.

22. McKercher, G.; Beaulieu, P. L.; Lamarre, D.; LaPlante, S.; Lefebvre, S.; Pellerin, C.; Thauvette, L.; Kukolj, G. Specific inhibitors of HCV polymerase identified using an NS5B with lower affinity for template/primer substrate. *Nucleic Acids Res.* **2004**, *32*, 422-431.

23. LaPlante, S. R.; Gillard, J. R.; Jakalian, A.; Aubry, N.; Coulombe, R.; Brochu, C.; Tsantrizos, Y. S.; Poirier, M.; Kukolj, G.; Beaulieu, P. L. Importance of ligand bioactive conformation in the discovery of potent indole-diamide inhibitors of the hepatitis C virus NS5B. *J. Am. Chem. Soc.* **2010**, *132*, 15204-15212.

24. Case, D. A.; Darden, T.A.; Cheatham III, T.E.; Simmerling, C.L.; Wang, J.; Duke, R.E.; Luo, R.; Merz, K. M.; Wang, B.; Pearlman D. A.; Crowley, M.; Brozell, S; Tsui, V.; Gohlke, H.; Mongan, J.; Hornak, V.; Cui, G.; Beroza, P.; Schafmeister, C.; Caldwell, J. W.; Ross W. S.; Kollman, P. A., **2004**, AMBER 8, University of California, San Francisco.

25. Duan, Y.; Wu, C.; Chowdhury, S.; Lee, M. C.; Xiong, G.; Zhang, W.; Yang, R.; Cieplak, P.; Luo R.; Lee, T. A Point-Charge Force Field for Molecular Mechanics Simulations of Proteins. *J. Comput. Chem.* **2003**, *24*, 1999-2012.

26. Jakalian, A.; Bush, B. L.; Jack D. B.; Bayly, C. I. Fast, Efficient Generation of High-Quality Atomic Charges. AM1-BCC Model: I. Method. *J. Comput. Chem.* **2000**, *21*, 132-146.

27. Wang, J.; Wolf, R.M.; Caldwell, J.W.; Kollman, P.A.; Case, D.A. Development and testing of a general Amber force field. *J. Comput. Chem.* **2004**, *25*, 1157–1174.

Table of Contents Graphic